Translational use of homing peptides: Tumor and placental targeting

DOI:
10.1016/j.jcis.2024.02.103

Document Version
Final published version

Journal of Colloid and Interface Science 662 (2024) 1033–1043

Contents lists available at ScienceDirect

Journal of Colloid And Interface Science

journal homepage: www.elsevier.com/locate/jcis

Translational use of homing peptides: Tumor and placental targeting

Abdulaziz A. Alobaid [a,b], Maximilian W.A. Skoda [c], Lynda K. Harris [a,d,e,f,*], Richard A. Campbell [a,*]

[a] Division of Pharmacy and Optometry, Faculty of Biology, Medicine and Health, The University of Manchester, Manchester M13 9PL, United Kingdom
[b] Department of Pharmaceutics, Faculty of Pharmacy, Kuwait University, P.O. Box 24923, Safat 13110, Kuwait
[c] ISIS Neutron & Muon Source, Rutherford Appleton Laboratory, Harwell Campus, Didcot OX11 0QX, United Kingdom
[d] Maternal and Fetal Health Research Centre, Division of Developmental Biology and Medicine, Faculty of Biology, Medicine and Health, The University of Manchester, Oxford Road, Manchester M13 9WL, United Kingdom
[e] St Mary's Hospital, Manchester University NHS Foundation Trust, Manchester Academic Health Science Centre, Manchester M13 9WL, United Kingdom
[f] Olson Center for Women's Health, University of Nebraska Medical Center, Omaha, NE 68198, United States

GRAPHICAL ABSTRACT

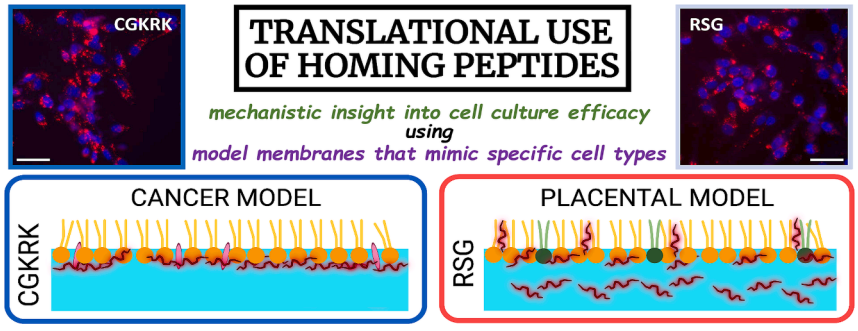

ARTICLE INFO

Keywords:
Homing peptides
CGKRK
RSG
Cancer
Tumor
Placenta
Cell cultures
Neutron reflectivity
Reflectometry

ABSTRACT

Hypothesis: Tissue-specific homing peptides have been shown to improve chemotherapeutic efficacy due to their trophism for tumor cells. Other sequences that selectively home to the placenta are providing new and safer therapeutics to treat complications in pregnancy. Our hypothesis is that the placental homing peptide RSGVAKS (RSG) may have binding affinity to cancer cells, and that insight can be gained into the binding mechanisms of RSG and the tumor homing peptide CGKRK to model membranes that mimic the primary lipid compositions of the respective cells.

Experiments: Following cell culture studies on the binding efficacy of the peptides on a breast cancer cell line, a systematic translational characterization is delivered using ellipsometry, Brewster angle microscopy and neutron reflectometry of the extents, structures, and dynamics of the interactions of the peptides with the model membranes on a Langmuir trough.

Findings: We start by revealing that RSG does indeed have binding affinity to breast cancer cells. The peptide is then shown to exhibit stronger interactions and greater penetration than CGKRK into both model membranes, combined with greater disruption to the lipid component. RSG also forms aggregates bound to the model membranes, yet both peptides bind to a greater extent to the placental than cancer model membranes. The results

* Corresponding authors.
E-mail addresses: lyharris@unmc.edu (L.K. Harris), richard.campbell@manchester.ac.uk (R.A. Campbell).

https://doi.org/10.1016/j.jcis.2024.02.103
Received 30 September 2023; Received in revised form 30 January 2024; Accepted 12 February 2024
Available online 13 February 2024

demonstrate the potential for varying local reservoirs of peptide within cell membranes that may influence receptor binding. The innovative nature of our findings motivates the urgent need for more studies involving multifaceted experimental platforms to explore the use of specific peptide sequences to home to different cellular targets.

1. Introduction

Breast cancer is a leading cause of mortality and the second most common cancer across the world [1]. In the United States, statistics show that in 2022 about 13 % of women will at some point in their lives be diagnosed with invasive breast cancer, and approximately 3 % will lose their lives [2]. Conventional chemotherapeutics, combined with radiotherapy or surgery offer great benefit in reducing the growth of tumors and improving the survival rates, but these therapies exhibit several drawbacks, such as poor pharmacokinetics, drug instability and, due to the systemic route of administration, they can act on both malignant and healthy cells leading to unwanted side effects [3]. Hence there is a pressing need to develop more selective delivery of chemotherapeutics to target tumor cells.

Targeted drug delivery can be achieved by creating nanoparticles decorated with moieties which bind to ligands that are expressed only on the surface of the target cell type. A number of studies have reported the use of monoclonal antibodies [4], aptamers [5], and homing peptides [6–8] to selectively deliver drugs to tumors.

Homing peptides are short, randomly occurring peptide sequences, often identified by biopanning techniques, that have the ability to bind to unique receptors expressed on the surface of cancer cells, angiogenic or remodeling blood vessels, or any healthy or diseased cell type of interest [9]. Examples of receptors that are exploited for tumor targeting include integrin αvβ3, αvβ5 and α5β1, which are overexpressed in tumor vasculature [6]. Coupling of these homing peptides to nanoparticles loaded with chemotherapeutics can create effective tumor treatments [10]. Internalization of homing peptides, or homing peptide-decorated nanoparticles is thought to occur through two methods: energy-dependent penetration mediated through translocation, and endocytic cellular uptake triggering one or more internalization mechanisms: macropinocytosis, clathrin-dependent endocytosis and caveolae-mediated endocytosis [11]. A new internalization pathway has been recently described for two tumor homing peptides CGKRK and CRGDKGPDC (iRGD), by which the uptake occurs through the CendR pathway [12].

CGKRK is a tumor homing peptide that was found to target tumor neovasculature in mouse models of breast cancer. The pentapeptide binds to the p32 protein, which is expressed on the surface of many cancer cell types [13]. Solid tumors and the developing placenta share common features such as elevated rates of proliferation, invasive behavior, inducing remodeling of the local vasculature and immune cell evasion [14]. We have shown that two previously published tumor homing peptides, CGKRK and iRGD, selectively bind to the uteroplacental vasculature and placental tissue in mice, and the outer syncytiotrophoblast layer of the human placenta [15]. By undertaking *de novo* screening experiments using phage display, we have also identified some novel placental homing peptide sequences [16,17], including RSGVAKS (RSG), which binds to the same target tissues. This is important because targeted delivery of drugs to the placenta represents a safer and more efficacious way of treating placental dysfunction underlying pre-eclampsia, fetal growth restriction and other pregnancy complications [18–20]. Nevertheless, RSG has not been demonstrated as a tumor homing peptide to date.

There is no framework to describe the mechanisms governing interactions of homing peptides with the lipid constituents of biological membranes [21]. Cell culture studies can help to quantify drug efficacy and nanoparticle uptake; however, they lack the ability to reveal mechanistic details of the interactions. The problem can be approached through studying interactions in model membrane systems. This is important, as although most homing peptides bind through receptors *in vivo* [15,22], there is clear evidence that the lipid composition of cell membranes affects the localization and signaling efficiency of anticancer drugs that function *via* receptor-mediated interactions [23,24], e.g., peptide binding can be affected by different lipids even of the same charge [25].

Model membranes allow researchers to investigate interactions at a molecular level, unravelling structural and compositional details on the amount of peptide bound to and located in the membrane [26]. Langmuir monolayers are widely studied as, although there is only one lipid leaflet, substrate interactions associated with supported lipid bilayers are circumvented without the need for challenging floating bilayers [27], and they are suitable for the application of the optical techniques ellipsometry and Brewster angle microscopy (BAM) as well as neutron reflectometry (NR) [28]. Such techniques have been used to good effect in various combinations to reveal mechanistic information about peptide–membrane interactions [29–32].

The aim of the present study is to gain mechanistic insight into the potential for translational use of homing peptides as therapeutics for distinct health conditions, achieved through a comparison of reflectometry data on interactions of homing peptides that bind to tumor and placental cells, with model membranes that mimic their lipid compositions.

Specifically, we start by revealing experimentally that the known placental homing peptide RSG can also home to breast cancer cells. Then we turn to interactions of two homing peptides, CGKRK and RSG, each with two different model membranes representing the primary lipid components of cancer (CAN) and placental (PLA) cell membranes. Peptide concentrations were used of 40 μM for cell binding, consistent with the range validated by our lab and others for imaging and cell culture studies [10,13,15,17], and 3 μM for model membranes, consistent with that validated for interactions of antimicrobial peptides with model membranes on the basis of their minimum inhibitory concentrations [28,29,33]. The CAN membrane consists of 1-palmitoyl-2-oleoyl-*glycero*-3-phosphocholine (POPC), 1,2-dioleoyl-*sn*-*glycero*-3-phospho-L-serine (DOPS) and cholesterol in a molar ratio of 6:2:2, respectively, while the PLA membrane consists of POPC, 1,2-dioleoyl-*sn*-*glycero*-3-phosphoethanolamine (DOPE) and sphingomyelin (SM) in the same respective molar ratio. The chosen components were informed by thin layer chromatography and mass spectrometry measurements of those in cell membranes of the breast cancer cell line MDA-MB-231 [34], and in isolated full term placental syncytiotrophoblast cells [35] combined with our decision to use 3 different lipids in each model: (1) to balance membrane complexity vs. instability, and (2) to retain sufficient differences between the models for resolution by the applied experimental techniques. The molecular ratio of 6:2:2 and starting surface pressure of 25 mN m^{-1}, close to the natural surface pressure of bilayers in cellular membranes [36], was informed by experiments designed to achieve stable model membranes, as described in section 1 of the Supporting Information.

While peptide–membrane interactions have been previously studied using different model platforms such as vesicles, monolayers on a Langmuir trough and supported lipid bilayers including various combined applications of reflectometry techniques [37], to the knowledge of the authors, the present work marks the first study with translational implications of the interactions of different homing peptides with tailored model membranes.

2. Materials and methods

2.1. Materials

Dulbecco's Modified Eagle Medium (DMEM), penicillin, streptomycin and glutamine solution were purchased from Sigma Aldrich (UK). Fetal bovine serum (FBS) was purchased from Invitrogen (UK). TrypLE express reagent was purchased from Gibco (UK). The human metastatic triple negative breast adenocarcinoma MDA-MB-231 (HTB-26™) was purchased from the American Type Culture Collection. The Hoechst 33342 nucleic acid stain was purchased from Invitrogen (UK). POPC, d_{31}-POPC, DOPE and DOPS were purchased from Avanti Polar Lipids (Germany) while SM, cholesterol and D_2O (99 % D) were purchased from Sigma Aldrich (UK). All lipids (99 %) were used as supplied. The peptides TAMRA-CGGGCGKRK (CGKRK) and rhodamine-RSGVAKS (RSG) were custom-made by Insight Biotechnology Ltd (UK). The net charges of CGKRK and RSG at pH 7 are +3 and +2, respectively (calculated using ref. [38]). It may be noted that the fluorescent tag was left on the peptides for ease of comparison of results from model membranes and cell cultures. Chloroform and ethanol were obtained from Fisher Scientific, UK. Ultrapure water was used in all experiments by passing deionized water through a Suez filtration unit (resistivity = 18.2 MΩ·cm).

2.2. Cell cultures

MDA-MB-231 cells were cultured in DMEM containing phenol red, supplemented with 10 % FBS and penicillin (100 IU/mL), streptomycin (100 μg/mL) and glutamine (2 mM). All cell culture experiments were performed in a 37 °C incubator with a 21 % oxygen/5 % CO_2 atmosphere. Culture medium was changed every 2–3 days until cells reached ~ 80 % confluence. For subculture, the culture medium was removed, and cells were washed twice with 10 mL preheated sterile PBS (pH 7.4) to remove any floating dead cells. TrypLE express reagent (3 mL) was added into the flask and incubated for 3 min to detach the cells. Cells were then centrifuged with 5 mL of serum containing medium at 1000 rpm for 5 min, and the pellet resuspended in 5 mL of culture medium. Cell counts were performed using an automated counter (Biorad, UK); cell viability was > 95 %. Images are shown in the text after 24 h and in section 2 of the Supporting Information after 1, 4 and 24 h.

2.3. Model membranes

Stock solutions of CGKRK and RSG were made by dissolving each powder in ultrapure water in a glass vial and applying a vortex for 5 min until completely dissolved. Final concentrations of 3 μM were then prepared by diluting the stock solution with ultrapure water prior to the start of or during injection for each experiment. Lipids mixture at 0.5 mg mL^{-1} for both the CAN and PLA model membranes were freshly made on the same day of each experiment. All experiments were performed at 21 ± 2 °C.

2.4. Langmuir trough

Surface pressure–area (π–*A*) measurements can provide information on thermodynamic properties such as phase transitions of lipid monolayers [28], as well as the extent of any drug interactions [39], where *A* is the average area per lipid molecule. The isothermal compressibility is a measure of the resistance to being compressed, and changes in the phase and orientation of the lipids result in changes in the reciprocal of compression modulus, C_s^{-1}, defined as

$$C_s^{-1} = -A\frac{d\pi}{dA} \quad (1)$$

Larger values mean that the membrane is more viscous [40]. Expected ranges for films are 12.5–50 mN m^{-1} in the LE phase and 100–250 mN m^{-1} in the LC phase [41].

Measurements were carried out for π–A isotherms, BAM and ellipsometry using a Kibron (Finland) G2 trough equipped with two Delrin barriers and placed on an anti-vibration table. Before starting all experiments, the trough was carefully cleaned with detergent, water, ethanol, and chloroform prior to use. The trough was then filled with 160 mL of ultrapure water and lipid solution (40 μL for CAN and 46 μL for PLA) was spread drop by drop onto the surface using a 100 μL Hamilton micro-syringe (USA). Following the spreading of the monolayer, and prior to the initiation of the compression, the lipid solution was left for 10 min to allow for solvent evaporation. Surface area compression was then initiated with a barrier speed of 20 mm min^{-1} using a metal alloy Wilhelmy plate as the pressure sensor, which was cleaned in a flame immediately prior to use. The plate was calibrated with reference to the forces experienced in air and pure water.

For the peptide experiments, the monolayer was first compressed to π = 27 mN m^{-1}, which over a few minutes relaxed to π = 25 mN m^{-1} prior to peptide injection, the result of which is referred to as a starting π = 25 mN m^{-1}. The surface area was then held constant by fixing the trough barriers in position. The peptide was then injected by hand into the subphase underneath the monolayer over a period of 15 s using a syringe with a bent 10-cm needle. This duration was shown to be as efficient as possible whilst not inducing mechanical disruption to the monolayer. The injection was performed by moving the tip of the needle over the entire area of trough, rather than keeping it at a single injection point, whilst the solution was expelled to encourage uniform distribution of the peptide solution and limit concentration gradients in the subphase. Then π was recorded with time. All the experiments were repeated twice to ensure the reproducibility of the measurements.

2.5. Fluorescence microscopy

For analysis by fluorescence microscopy, MDA-MB-231 breast cancer cells were seeded in a 24 well plate containing sterile 18 mm glass cover slips, at a density of 5×10^4 cells/well and incubated overnight at 37 °C. 40 μM CGKRK- and RSG-labelled peptides were incubated with the cells for 24 h. Before imaging, the media was aspirated, and the cells were washed twice with pre-warmed PBS buffer. Cells were then stained with Hoechst 33342 dye (5 μM/ml, 5 min, 37 °C) and washed with 1× PBS. Images were acquired using a fluorescent inverted microscope (Leica DMI6000, Leica Microsystems, UK) coupled with a 5.5 Neo sCMOS camera (Andor, UK). Fluorescence of the TAMRA/rhodamine-labelled peptides was detected using an emission band pass filter of 575 ± 25 nm. The μManager software (v.1.46, Vale Lab, UCSF, USA) was used for image capture; images were viewed using ImageJ 1.53v software.

2.6. Ellipsometry

Ellipsometry is a highly sensitive optical technique used in characterizing thin film properties [42]. The change in polarization of light reflected off a lipid model membrane at the air/water inteface can give information about its dielectric properties. While measurements at the solid/liquid interface can be sensitive to the amplitude change, Ψ, and phase shift, Δ [43], the change in Ψ is often minimal for thin films at the air/water interface, and only changes in Δ are used in data interpretations [44]. Here a measure of the phase shift resulting from lipid and peptide in the monolayer is expressed as, defined as

$$\Delta_{surf} = \Delta_{layer} - \Delta_{water} \quad (2)$$

where Δ_{layer} is the measured value, and Δ_{water} is that of pure water. The magnitude of Δ_{surf} may be taken as a measure of the total interfacial thickness including peptide binding, and temporal fluctuations can reveal lateral heterogeneity such as binding domains or induced lipid phase separation [44]. Data were recorded using a Nanofilm EP4 instrument (Accurion, Goettingen, Germany) with a blue diode laser (489

nm), an angle of incidence of 50°, and a data acquisition rate of 0.1 Hz. Values of Δ_{surf} are presented, where the subtraction of Δ_{water} from pure water helps to reduce the impact of surface roughness on the data and corrects for small, systematic errors that may be caused by instrument drift and deflector positioning during calibration of the experiments.

2.7. BAM

BAM is an optical imaging technique used to examine the lateral morphology of the peptide interactions with lipid monolayers [45]. Both the anisotropy associated with LC domains and domains from binding to lipid monolayer result in higher reflectivity, manifested as brighter regions.

BAM images were recorded using the same Nanofilm EP4 instrument (Accurion, Goettingen, Germany), which was mounted on top of the G2 trough. The instrument was equipped with a blue diode laser (489 nm), a polarizer, an analyzer, a 10× magnification objective lens and a CCD camera. Without consideration of surface roughness effects, the reflectivity of p-polarized light at the Brewster angle of the air/water interface (53.1°) is nil. Therefore, any changes in the refractive index profile across the interface will result in increased reflection. BAM images were first taken for the lipid membrane before peptide injection into the subphase, and then they were taken at different time points following the injection. The background was subtracted from the images using an automatic feature of the instrument software with image focusing enabled. Consistent gamma correction was then applied to all the images equivalently (Irfanview v4.54, Germany).

2.8. NR

NR is an interfacial technique that allows resolution of the composition and stratified layer structures on the Å-scale, thanks to the use of isotopic substitution [46,47]. The reflectivity, R, is measured as a function of the momentum transfer normal to the interface, Q_z, defined as [48]

$$Q_z = \frac{4\pi \sin\theta}{\lambda} \tag{3}$$

where θ is the incidence angle and λ is the neutron wavelength. Experiments were conducted using troughs of dimensions 220 × 50 mm. Each trough was filled with 30 mL, 3 μM peptide solution, and a pre-calibrated volume of lipid solution of 32 μL (CAN) or 34 μL (PLA) was spread dropwise on the surface using a Hamilton syringe to form the model membranes at an equivalent starting π of 25 mN m^{-1}. These volumes were pre-calibrated as those required to reach π = 25 mN m^{-1} for the membranes on a pure water subphase in the absence of peptide, hence equivalent to a starting π = 25 mN m^{-1} for an injection experiment. Different methodology to peptide injection was motivated by a reduction in equilibration time due to peptide diffusion, given the precious nature of beam time, and as a direct result reduced experimental variability.

Specular NR measurements were performed on the time-of-flight reflectometer INTER at the ISIS Neutron and Muon Source (Didcot, UK). Two grazing incident angles of 0.8° and 2.3° and a wavelength range of λ = 1.5–16 Å were used. The absolute reflectivity, defined as the ratio of the number of neutrons in the specular reflection divided by those in the incident beam, was calibrated using pure D_2O. The fully accessible Q_z-range = 0.01–0.25 $Å^{-1}$ was recorded to resolve the structure of CGKRK or RSG with CAN or PLA membranes in 4 isotopic contrasts: fully hydrogenous lipid mixtures or those involving d_{31}-POPC, each on D_2O or on a mixture of 8.1 %v/v D_2O in H_2O that is invisible to neutrons called air contrast matched water (ACMW). The background was subtracted from the data using the area detector.

The data were analyzed using Motofit [49], with co-refinement of the global fit of a model comprising stratified layers to the data from different isotopic contrasts to minimize the global χ^2 value, and stated uncertainties corresponding to the range of values that result in a 10 % increase in global χ^2. For each layer, i, four parameters were used for its characterization: the scattering length density (SLD), the thickness (d_i), the roughness and the solvent volume fraction (φ_i). Residual background values were used consistently, as follows: 1.1×10^{-5} for measurements in ACMW and 6.3×10^{-6} for measurements in D_2O. A roughness value of 3.5 Å, consistent with the presence of capillary waves [50], was applied to all interfaces. A general procedure was followed of fitting data using a structural model that has the minimum number of fitting parameters required, together with principles such as preserving physical reality by constraining the surface excesses of lipid chains and headgroups to be equal, as described in a recent article on modelling neutron reflectivity data of monolayers at the air/water interface [51].

In the absence of peptide, the thickness of layer 1 was fitted as 12.3 ± 0.4 Å and 13.2 ± 0.6 Å for CAN and PLA, respectively. The thickness of layer 2 was fixed to 8 Å for CAN membrane and 6 Å for PLA membrane, determined iteratively to be the optimum values, to reduce the number of free fitting parameters.

In the presence of peptide, the global fit of the full Q_z data was performed first by considering a model comprising only two layers of lipid chains (layer 1) and lipid headgroups and solvent (layer 2) where the amount of peptide in each layer was fitted iteratively. Where appropriate, an additional layer of peptide and solvent was added (layer 3). For the same reason of minimizing the number of free fitting parameters, the thickness of layer 3 was fixed at 20 Å with the solvent volume fitted, although it was allowed to vary with respect to the isotopic contrast to account for isotope-specific effects. In three out of the four investigated systems – CAN-RSG, PLA-CGKRK and PLA-RSG – the increase in global χ^2 was highly significant when neglecting the presence of layer 3, which evidenced the need for this extra layer comprising only solvated peptide. This point is elaborated below.

The surface excess of component i, Γ_i, in a layer can be obtained through the following equation:

$$\Gamma_i = \frac{\mathrm{SLD} \bullet d \bullet \varphi_i}{\Sigma b_i \bullet N_A} \tag{4}$$

where φ_i is its volume fraction in a layer of thickness d, Σb_i is its scattering length and N_A is Avogadro's number.

3. Results

3.1. Cell cultures (fluorescence microscopy)

We and others have previously demonstrated that the tumor homing peptide CGKRK binds to the surface of cancer cells [13] and the placenta [15]. Here we demonstrate for the first time that the novel placental homing peptide sequence RSG [16] also has the capacity to bind to cancer cells. Incubation of the human breast cancer cell line MDA-MB-231 with 40 μM of the fluorophore-tagged peptides CGKRK and RSG for 24 h led to spontaneous cell surface binding and internalization of both sequences, as shown in Fig. 1A. Individual cells are identified by the nuclear stain Hoechst 33342, shown in blue. Both peptides, shown in red, have accumulated within the cytoplasm of the cells, as evidenced by the punctate areas of fluorescence surrounding the nuclei. Images shown in section 2 of the Supporting Information feature shorter incubation times of 1 and 4 h, indicating that the interactions begin even over the shorter exposure times associated with the model membrane experiments described below. To deepen our understanding of how these peptides interact with their target cell membranes, here we undertake a novel mechanistic study to unravel the mechanisms underlying the binding process of these peptides to two distinct types of cell membranes, which were designed to mimic the key lipid components that have been identified in cancer and placental cells.

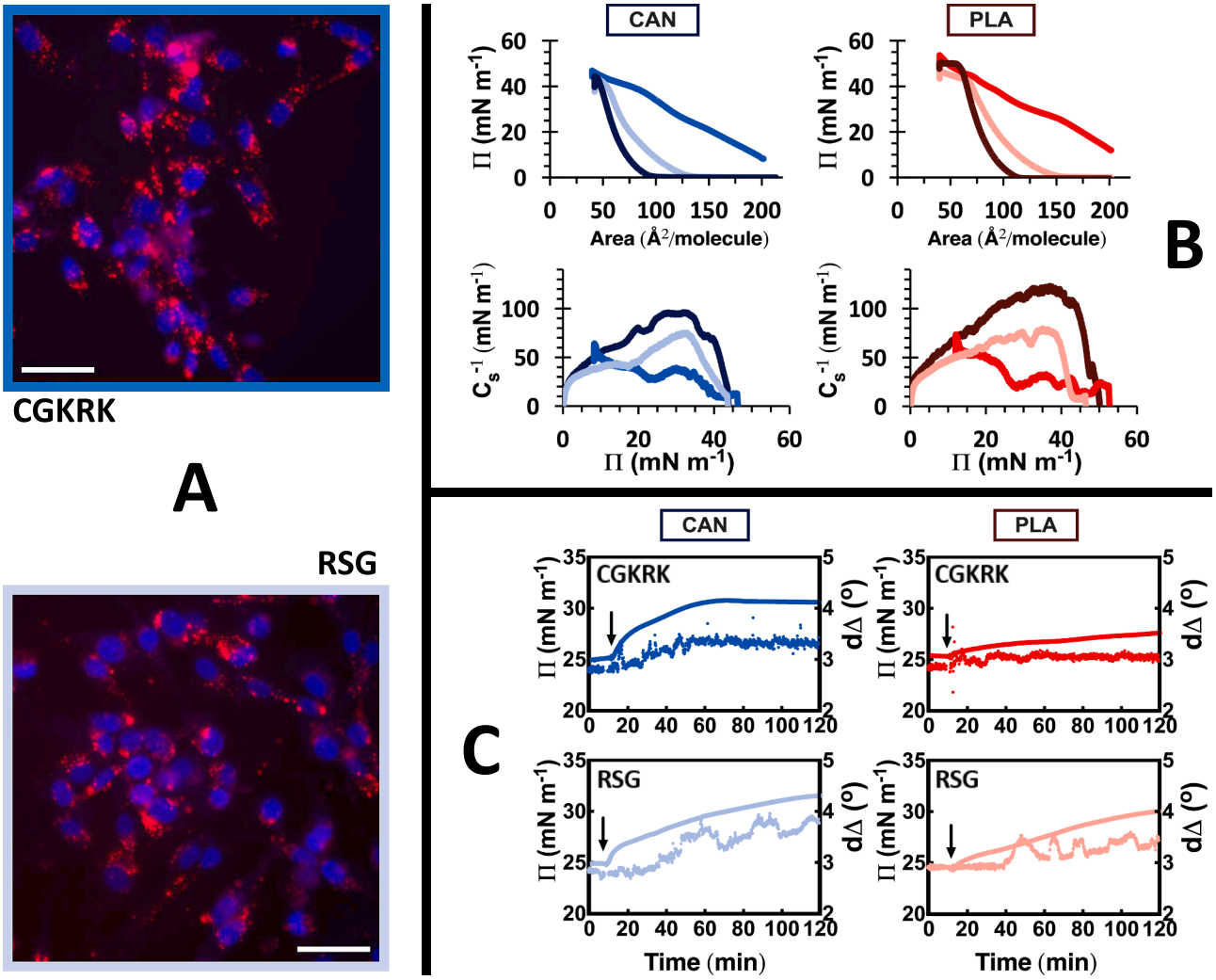

Fig. 1. (A) Binding of the tumor homing peptide TAMRA-CGKRK or and the placental homing peptide rhodamine-RSG to the triple negative breast cancer cell line MDA-MB-231 at a concentration of 40 μM after 24 h. Nuclei were stained with Hoechst 33342 shown in blue; peptides are shown in red; scale bars = 50 μm. (B) π–*A* isotherms and C_s^{-1} of the monolayer (dark blue/dark red) or following exposure of 3 μM CGKRK (blue/red) or RSG (light blue/light red), as a function of *A* for CAN (left) and PLA (right). (C) Changes in π and Δ_{surf} of CAN (left) and PLA (right) exposed to a final concentration of 3 μM CGKRK (blue/red; top) or RSG (light blue/light red; bottom); black arrows indicate injections. (For interpretation of the references to colour in this figure legend, the reader is referred to the web version of this article.)

3.2. π–*A* isotherms (Langmuir trough)

Fig. 1B shows π–*A* isotherms (top) and C_s^{-1} (bottom) of the model membranes in the absence or presence of 3 μm CGKRK or RSG, where the cancer model membrane (hereafter called 'CAN') features in the left panels. In the absence of peptide, the π lift-off, where the monolayer transitions from the gas to the liquid expanded (LE) phases, is at ~ 90 Å^2/molecule. Upon compression, π rises until monolayer collapse at 43 mN m^{-1}, which is qualitatively consistent with results from a study on a monolayer where POPC was substituted for 1,2-dipalmitoyl-*sn*-*glycero*-3-phospho-choline (DPPC), which exhibited similar properties and collapse at 46.5 mN m^{-1} [40]. A value of C_s^{-1} = 90 mN m^{-1} is observed at π = 25 mN m^{-1} (noted for reference below), close to the liquid condensed (LC) phase, with a maximum of 96 mN m^{-1}.

As a result of exposure of CGKRK from the subphase to CAN, the π–*A* isotherm shows a marked increase in the π lift-off to >200 Å^2/molecule, indicative of strong peptide–membrane interactions. An inflection is observed at *A* = ~140–100 Å^2/molecule, as mirrored in C_s^{-1} at ~25–30 mN m^{-1}. The starting π is 8 mN m^{-1}, and the value rises sharply upon compression until it reached the collapse π of 47 mN m^{-1} (higher than that of CAN). Lower values of C_s^{-1} are associated with interactions of CGKRK with CAN with C_s^{-1} = 35 mN m^{-1} at π of 25 mN m^{-1}, and a maximum C_s^{-1} of 73 mN m^{-1}, on the borderline of those corresponding to LE and LC phases, hinting at a fluidizing effect of the peptide–membrane interaction. This result suggests that the peptide interactions modify the phase of the model membrane. Exposure of RSG to CAN results in an intermediate π–*A* isotherm with a π lift-off of ~130 Å^2/molecule, a gradual increase in π, and a similar collapse π of 45 mN m^{-1}. Generally, the CAN interactions of RSG exhibit even lower C_s^{-1}, e.g., just 62 mN m^{-1} at π = 25 mN m^{-1} (> 30 % reduction), suggesting a more strongly fluidizing nature of RSG in its membrane interaction.

Analogous data on the placental model membrane (hereafter called 'PLA') feature in the right panels of Fig. 1B. In the absence of peptide, the π lift-off of PLA is higher than that of CAN at ~110 Å^2/molecule with higher collapse at π = 50 mN m^{-1}. PLA has a C_s^{-1} value of 103 mN m^{-1} at π = 25 mN m^{-1} with a maximum of 123 mN m^{-1}, showing that the monolayer is in the LC phase.

Observations of the interactions of CGKRK and RSG with PLA are qualitatively like those with CAN, with a commensurate reduction in C_s^{-1}, although the collapse π for CGKRK is even higher at 54 mN m^{-1}. Additionally, the π–*A* isotherm with CGKRK displays inflections at *A* = ~150–100 and 75–50 Å^2/molecule, mirrored at C_s^{-1} = 25–35 and

35–43 mN m^{-1}, respectively. Such inflections when peptide is present can be attributed to changes in the orientation or organization of the peptide or lipid molecules.

The results indicate that interactions of CGKRK are stronger than those of RSG with both CAN and PLA. However, such an interpretation is reliant on an *a priori* assumption of negligible (or equivalent) lipid loss from the model membrane, which has been shown experimentally in other systems not to be valid.[29,52] Also, the inference seems inconsistent with the more fluidizing effects of RSG than CGKRK. Such effects on C_s^{-1} are more pronounced for CAN than PLA at $\pi = 25$ mN m^{-1}. Additional techniques to elucidate the interactions are applied below.

3.3. Interaction extent and heterogeneity (ellipsometry)

Fig. 1C shows time-resolved measurements of π and Δ_{surf} of the model membranes (starting $\pi = 25$ mN m^{-1}) up to 2 h following injection into the subphase to a final concentration of 3 μM CGKRK or RSG, where CAN features in the left panels. Changes in the parameters initially and at longer times give insight into the rates and extents of interactions of the peptides with the model membranes. Interactions of CGKRK with CAN result in a pronounced increase in π of 3 mN m^{-1} in the first 15 min after injection with the values increasing to a maximum of 31 mN m^{-1} after 1 h. The behavior is mirrored by a gradual increase in the mean value of Δ_{surf} of 13 % over the same period. These rises are attributed to interactions of the positively charged peptide with the negatively charged phosphoserine component of CAN. Even so, the interactions of RSG with CAN are distinct. The rise in π after peptide injection is less pronounced with an increase of <2 mN m^{-1} in the first 15 min, yet the values rise to the same maximum, and increase in the mean value of Δ_{surf} over the same period is almost double at 22 %. There are also temporal fluctuations in Δ_{surf} on the minute time scale, indicating domains from lipid phase separation or peptide binding [53].

Analogous data on PLA feature in the right panels of Fig. 1C. CGKRK does not induce as significant a change in π on PLA, compared with that on CAN, with values rising just 1 mN m^{-1} in the first 15 min followed by a further slow increase to 28 mN m^{-1} after almost 2 h. A relatively small increase in the mean value of Δ_{surf} of 6 %, in keeping with this result, suggests reduced peptide–membrane interactions, which may be explained by the absence of negatively charged lipid in this membrane, and that CGKRK favors electrostatic interactions [54]. Interactions of RSG with PLA are also more gradual than those with CAN, but in this case pronounced temporal fluctuations over a time scale of several minutes suggest more substantial discrete regions of peptide binding or induced lipid phase separation because of the interaction combined with higher film rigidity. Such a result may initially seem inconsistent with the more fluidizing nature of RSG than CGKRK on the model membranes inferred above from Cs^{-1}, but the higher rigidity of the membrane revealed by ellipsometry can be related to domains of bound peptide. The reduced interactions of both peptides with PLA can be attributed to the absence of negatively charged lipids in the model membrane.

The data taken together show that, regardless of the peptide, interactions with CAN are initially more pronounced, probably due to electrostatic interactions with the negatively charged lipid component of the model membrane, while interactions with PLA are characterized by more modest and gradual changes. On the other hand, the overall increase in the average values of Δ_{surf} with both model membrane systems is about double for RSG than for CGKRK, and pronounced but slow fluctuations indicate a pronounced lateral heterogeneity and high film rigidity of PLA. We go on now to discuss optical images from BAM prior to structural characterization of the systems using NR.

3.4. Interfacial morphology (BAM)

Fig. 2 shows representative time-resolved images of the model membranes (starting $\pi = 25$ mN m^{-1}) at 10 and 30 min after injection into the subphase to a final concentration of 3 μM CGKRK or RSG, while images of CAN and PLA at $\pi = 25$ mN m^{-1} in the absence of peptide, as well as enlarged images of those shown and ones recorded at an additional time after injection can be found in section 3 of the Supporting Information. At $\pi = 25$ mN m^{-1}, CAN exhibits a distribution of faint spots, indicative of the phase-separating effect of cholesterol [55], combined with the borderline LE–LC nature of the membrane discussed above. PLA, on the other hand, displays a smaller number of brighter spots, consistent with its higher C_S^{-1} at $\pi = 25$ mN m^{-1} taking the membrane into the LC phase. Binding of CGKRK to either membrane results in rapid disruption (within 10 min) of the faint anisotropic domains after the interaction, and no further changes are evidenced up to 30 min. RSG, on the other hand, has a minimal effect on CAN and a much greater effect on PLA. In the latter case, binding of RSG results in the transient presence of bright domains, coincident with the short-lived rise in π, before the features become slightly larger and less bright in appearance (between 10 and 30 min), coincident with the disruptive and fluidizing effect of these peptide interactions. This mechanism exhibits similarities to that resolved in other peptide–membrane studies [29,52]. Clearly, RSG interactions with PLA are distinct in their membrane-binding, so NR was used to provide further insight.

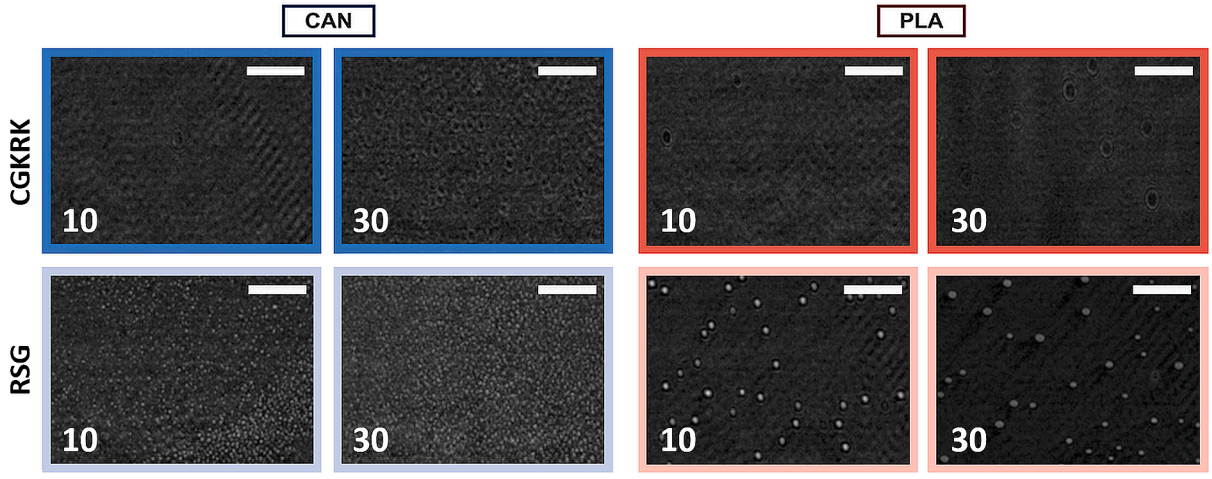

Fig. 2. BAM images of CAN (left) and PLA (right) membranes exposed to 3 μM CGKRK (blue/red borders; top) or RSG (light blue/light red borders; bottom) at the different interaction times indicated in minutes; scale bars = 100 μm. (For interpretation of the references to colour in this figure legend, the reader is referred to the web version of this article.)

3.5. Membrane binding structure (NR)

NR measurements were performed initially to resolve reference structures of CAN and PLA at $\pi = 25$ mN m^{-1}. The fixed structural parameters used are shown in section 4 of the Supporting Information, while the reflectivity data, model fits and volume fraction profiles are presented in section 5. It may be noted that the surface excess of both lipid monolayers is 2.32 ± 0.12 μmol m^{-2}, equivalent to $A = 71 \pm 2$ Å^2.

To resolve the composition and structure of CAN and PLA exposed to CGKRK or RSG, neutron reflectivity profiles were recorded in 4 isotopic contrasts: the hydrogenous lipid mixtures or those involving d_{31}-POPC, each on D_2O or ACMW. The data were fitted using a three-layer model: layer 1 of lipid acyl chains in the absence or presence of peptide, layer 2 of solvated head groups in the presence of peptide, and layer 3 – where required – of solvated peptide. This model was based on the similar ones described in the literature that account for the binding of peptides to lipid monolayers [29,52]. For the systems that required the presence of layer 3, the increase in global χ^2 averaged at 75 % for the corresponding optimized fits in its absence: the fits and global χ^2 values are reported in section 6 of the Supporting Information. The use of isotopic contrast variation involving lipid chains with mean scattering length densities of 1.99×10^{-6} Å^{-2} (CAN involving d_{31}-POPC) vs. -0.20×10^{-6} Å^{-2} (CAN), and 1.78×10^{-6} Å^{-2} (CAN involving d_{31}-POPC) vs. -0.28×10^{-6} Å^{-2} (CAN), as well as solvent with scattering length densities of 6.36×10^{-6} Å^{-2} (D_2O) vs. 0 Å^2 (ACMW), provides sufficient resolution to determine the location of the peptide within the model membranes.

Fig. 3 shows the neutron reflectivity data, model fits and volume fraction profiles. Data are displayed on a scale of RQ_z^4 vs. Q_z, and analogous data on a scale of log(R) vs. Q_z are shown for comparison in section 7 of the Supporting Information, while a summary of the fitted structural parameters can be found in section 8. Where present in a layer bound below the lipid head groups, the peptide volume fraction varies according to the isotopic contrast of the solvent, which we attribute to isotope-specific effects that have been reported previously for peptide and protein systems [56], and mirror effects resolved in extended layers of polymer/surfactant mixtures [57]. As ACMW contains < 10 %v/v D_2O (i.e. much closer than D_2O to the isotopic composition of pure water), as an approximation, remarks on the interfacial structures below relate to the structures resolved in ACMW.

For exposure of CAN to CGKRK, the thickness of the lipid acyl chains (layer 1) is 11.5 ± 0.5 Å while that exposed to RSG is equivalent at 11.6 ± 0.7 Å. The amount of CGKRK bound to the membrane is 0.22 ± 0.04 μmol m^{-2}, associated entirely among the lipid head groups (layer 2); addition of layer 3 comprising solvated peptide did not improve the fit quality. The bound amount of RSG is much higher than CGKRK at 0.75 ± 0.11 μmol m^{-2} with 13 % associated with the lipid acyl chains (layer

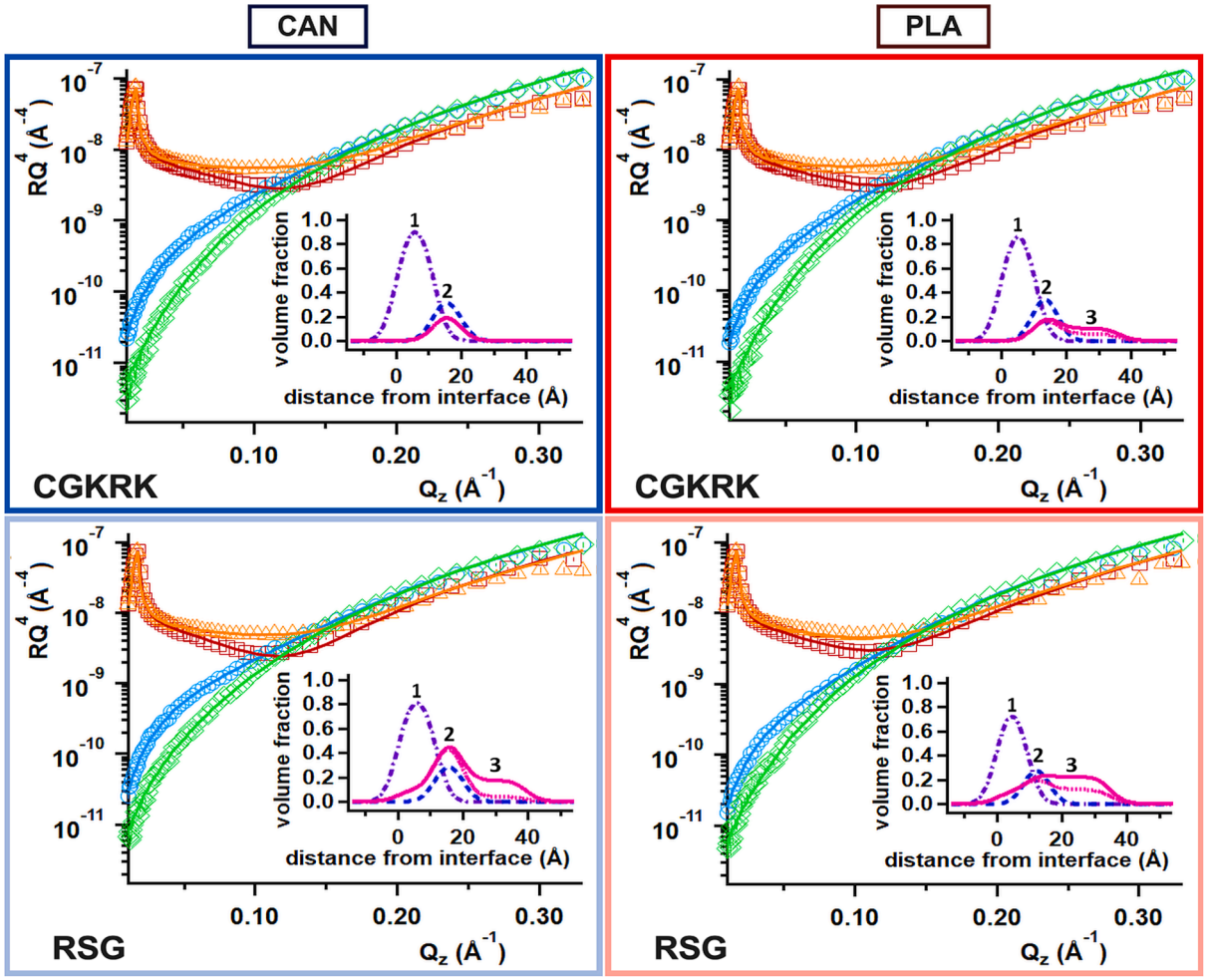

Fig. 3. Neutron reflectivity profiles for CAN (left) and PLA (right) exposed to 3 μM CGKRK (blue/red borders; top) or 3 μM RSG (light blue/light red borders; bottom) with lipid spread to a starting $\pi = 25$ mN m^{-1}, involving CAN or PLA on ACMW (green diamonds) and on D_2O (orange triangles), and CAN or PLA involving d_{31}-POPC on ACMW (blue circles) and on D_2O (red squares); optimized fits are shown as solid lines with matching colors for each contrast. Volume fraction profiles are shown as insets: lipid chains (purple dotted-dashed lines) and head groups (dark blue dashed lines), and peptide in ACMW (pink solid lines) and in D_2O (pink dotted lines), where layers 1, 2 and 3 in the model are indicated. (For interpretation of the references to colour in this figure legend, the reader is referred to the web version of this article.)

1), 50 % among the lipid head groups (layer 2), and 37 % bound below them (layer 3). Comparison of the two systems reveals that RSG displaces more lipid than CGKRK: there is 16 % loss for RSG compared with 6 % for CGKRK (resulting in 1.96 ± 0.10 and 2.17 ± 0.10 μmol m^{-2}, respectively). Clearly, RSG causes much more disruption to the membrane with deeper penetration.

For exposure of PLA to CGKRK, the thickness of the lipid acyl chains (layer 1) is 10.4 ± 0.6 Å while that exposed to RSG is slightly lower at 9.1 ± 0.7 Å. The total amount of CGKRK bound to PLA is less than to CAN at 0.29 ± 0.09 μmol m^{-2}, with 59 % of it associated among the lipid head groups (layer 2) and 41 % bound below them (layer 3). The bound amount of RSG is greater at 0.58 ± 0.12 μmol m^{-2} with 14 % associated with the lipid acyl chains (layer 1), 22 % among the lipid head groups (layer 2), and 64 % bound below them (layer 3). These results show reduced penetration of the peptides with PLA than CAN, i.e., into the acyl chains for CGKRK and the head groups for RSG. As observed with CAN, RSG displaces more lipid than CGKRK with PLA: there is 38 % loss for RSG compared with 22 % for CGKRK (resulting in 1.44 ± 0.10 and 1.82 ± 0.10 μmol m^{-2}, respectively). These results show that both peptides cause more disruption of PLA than CAN, again with RSG being the more disruptive.

4. Discussion

The present study was designed to resolve the interactions of the CGKRK and RSG peptides with two different model membranes mimicking the primary lipid compositions of cancer and placental cells. While CGKRK was identified as a tumor homing peptide [13], there is recent evidence that it also binds to the placenta [15]. RSG binds to the placenta and the uteroplacental vasculature [16], yet our first result was to provide new evidence that RSG can also act as a tumor homing peptide, before we turned to the model membranes for mechanistic insight. Data from π–*A* isotherms with compression modulus, BAM, ellipsometry and NR were acquired on the interactions of CGKRK or RSG with the CAN or PLA membranes, with the expectation that useful information could be obtained on different time and length scales. We hypothesized that the results would validate a platform for future research on other homing peptides. To aid this discussion, Fig. 4 depicts the association of CGKRK and RSG with both model membrane systems, noting that the presentation is purely illustrative. Let us consider the interactions of each peptide in turn.

CGKRK was previously reported to exhibit fast penetration into the human placental membrane and accumulates intracellularly in 5–15 min [15]. The results of the present study show that the extent of interaction of CGKRK is higher with the CAN than the PLA membranes. The values of π rise rapidly by 5 mN m^{-1} in the first 20 min, as opposed to by just 1.5 mN m^{-1}, for the two respective systems. This difference is attributed to strong electrostatic interactions between the peptide and the negatively charged phosphoserine groups present only in the CAN membrane. CGKRK has an overall positive net charge of +3 as it composed of the basic residues lysine (K) and arginine (R) [54]. NR data have revealed that CGKRK is solely associated with the lipid head groups of the CAN membrane, while it is split equally between association among the lipid head groups and bound below them for the PLA membrane. No CGKRK was detected in the acyl chains layer in either model membrane. Ellipsometry data have revealed that CGKRK interactions result in a change in Δ_{surf} of 13 % and 6 % for the CAN and PLA membranes, respectively, indicating reduced formation of condensed domains, while the images recorded with BAM show no visible formation of condensed domains. Taken together, these results show that CGKRK associates mainly with the head groups due to the electrostatic interactions between the peptide and the membrane and might be

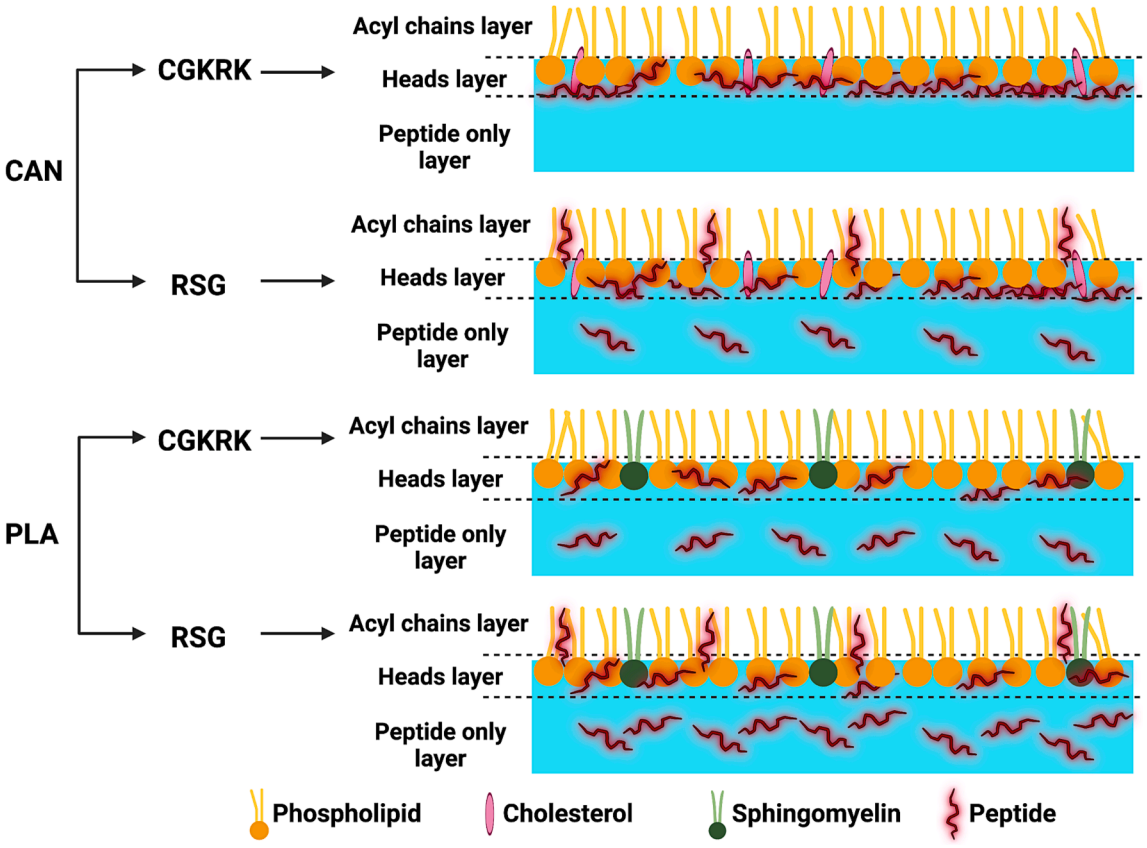

Fig. 4. Schematic of interfacial structures formed from interactions of CGKRK or RSG peptides with model cancer (CAN; top) and placental (PLA; bottom) cell membranes.

segregated into lateral domains below the membrane. Such segregation can explain the rise in π–*A* isotherm obtained with the compression modulus, as was also noted in a recent study on drug interactions [58].

RSG also exhibits pronounced binding activity to the CAN membrane, which may also be attributed to the same electrostatic interactions. Surprisingly, however, although the initial rise in π is slower for its interactions with both membrane types, the overall increases in π are higher than for CGKRK after 2 h (6.5 and 5 mN m^{-1} for RSG, versus 5.5 and 2.5 mN m^{-1} for CGKRK, with the CAN and PLA membranes, respectively). NR data has revealed that 15–20 % of RSG penetrates the acyl chains in both systems. In the CAN membrane, most of the peptide is associated among the head groups (50 % in the ACMW contrast that is close in isotopic composition to pure water) with the remaining amount (37 %) bound below them. The interactions of the peptide among the head groups of the PLA membrane were reduced, with 22 % in ACMW associated among the head groups and the remaining 48 % bound below them. Ellipsometry data have revealed that RSG results in a higher final change in Δ_{surf} of 22 % and 12 % for CAN and PLA, respectively, approximately double the changes seen with CGKRK. BAM images have revealed small brighter spots in both membranes, which could be explained as the penetration of the peptide into the acyl chains of the membranes, as evidenced with NR. Taken together, these results suggest the strong potential of RSG to penetrate both types of model membranes studies, and it supports its newly demonstrated efficacy in interacting with cancer cell membranes.

Cell penetrating peptides (CPPs) are a type of peptides that can bind to and translocate into biological membranes in an energy- and receptor-independent manner [59,60]. A number of CPPs peptides have been reported in the literature to have the ability to spontaneously penetrate biological membranes such as TAT (GRKKRRQRRRPQ) and penetratin (RQIKIWFQNRR-MKWKK) [61]. Indeed, both CGKRK and RSG exhibit cell penetrating behavior *in vitro* and *in vivo* [10,15,16]. As seen with both membrane types in the present work, CGKRK predominantly associates among the lipid head groups, which in the lipid bilayer of a cell membrane would be oriented to the outside and inside of the cell (not the inner body of the membrane). Since CPPs are known to bind spontaneously to and internalize through the cell membrane, our results support inference that in cancer cells CGKRK may bind to the membrane surface, and/or penetrate through it, but would be less likely to embed within it. In contrast, RSG has been shown to bind not only to the lipid head groups but also penetrate the lipid chains of both membrane types, implying potentially stronger binding and membrane insertion in biological systems, providing a sink for receptor interactions.

5. Conclusions

In the present work, we have evidenced the ability of a novel placental homing peptide, RSG [15], to bind to cancer cells, and have shown for the first time the nature and extent of its interactions, and those of the tumor homing peptide CGKRK [13], with two model membranes representing the primary lipid components of cancer and placental cell membranes. In biological systems, cell membranes display different receptors on their surface, which may represent potential target receptors for homing peptides [62]. However, a number of membrane-interacting peptides have been reported in the literature that bind to, and penetrate, lipid bilayers, and are capable of efficient translocation [37]. Moreover, when considering conditions where the peptide is in excess, or the spatial arrangement of nanoparticles decorated with multiple copies of a targeting peptide [63], not every peptide will interact with cell surface receptors, but will interact with the local lipid environment.

The peptides studied display faster binding to the negatively charged CAN membrane, as shown by the time-resolved increase in π. While CGKRK exhibits faster interactions with the CAN membrane in the first 30 min, RSG results in higher Δπ after 2 h. A similar interaction rate was observed for RSG with the PLA membrane, yet the Δπ change is higher than that of CGKRK. The morphological changes observed with BAM reveal brighter dots, indicative of domains of lipids in the LC phase, for RSG in both membranes, in contrast to CGKRK where no apparent phase separation is observed, suggesting a greater degree of disruption of the membrane structure by RSG than by CGKRK. This inference was further validated by ellipsometry, where the overall changes in Δ_{surf} for RSG with both membranes are almost double those for CGKRK, indicating the existence of reorganized, thicker domains. NR data has shown the ability of RSG to penetrate the acyl chains region and bind into the head groups of both membranes, with most of the peptide attributed to being associated with the charged head groups of the CAN membrane, while CGKRK was found to be solely bound to the head groups of both membranes.

Both peptides have been resolved to have mechanisms of action that categorize them as CPPs [59,60]. Indeed, biologically, CGKRK is classified as a CPP that contains the highly basic KRK sequence that is common to many CPPs [64,65]. However, it should be cautioned that either peptide may exhibit different association and internalization mechanisms in cellular systems. Also, the more superficial interactions of CGKRK with the model membranes are unlikely to impede binding to its target cell surface receptor (p32 in cancer cells [13] and calreticulin in the human placenta [15]) and interfere with receptor-mediated tissue targeting. As CGKRK penetrates the PLA membrane to a lesser extent than the CAN membrane, it may be that it exhibits faster receptor-mediated binding and internalization in placental cells than tumor cells; however, direct comparisons of these biological systems are yet to be explored. The tumor homing peptide CGKRK displays a moderate extent of interaction with model membranes representing both cancer and placental cell membranes. As a stronger extent of interaction between RSG with the CAN than PLA membranes has been demonstrated, the potential application of RSG as an effective CPP in cancer cells is endorsed, which supports our new finding using breast cancer cells that RSG acts as a tumor homing peptide.

We have presented in this work a demonstration of how known homing peptides may interact with the model membranes of their target cells. Our approach involves the use of experiments on cell cultures and model membranes, the latter studied on a Langmuir trough using reflectometry techniques applied over a range of time and length scales. Our approach sits alongside others such as the use of reflectometry techniques on solid support lipid bilayers [66] or translocation studies through droplet interface bilayers [67]. It may be commented that a strength of our approach is the combination of insight gained into peptide efficacy with their mechanisms of interactions, while a limitation is the different time scales over which techniques need to be applied (given their experimental requirements), with cell culture measurements typically requiring several hours or even more than a day and model membrane measurements often being much shorter [68,69].

In summary, our approach had validated an experimental platform suited to the investigation of a broad range of other homing peptides and CPPs [70]. Indeed, the need for rational design of precision nanoparticles, particularly for use in pregnancy, is now being recognized [71]. Commonly used model systems to study CPP interactions with lipid membranes include different sizes of unilamellar and multilamellar vesicles, although such investigations are all hampered by light scattering [72]. Our innovative approach offers an alternative way to study homing peptide–membrane interactions, which can be exploited to predict peptide behavior, inform the design of customized nanoparticle formulations, and used as a screening method to select the most efficacious CPPs for the cell or tissue of interest. Indeed, potential has been demonstrated for such a multifaceted approach to help develop the most effective targeted therapies through cell culture and *in vivo* experiments.

6. Associated content

Supporting Information available with the following sections: (1) surface pressure stability study, (2) fluorescence microscopy images at

different incubation times (3) additional and enlarged BAM images, (4) NR fixed structural parameters, (5) NR data, fits and parameters of CAN/PLA membranes, (6) NR data alternative fits and global χ^2 values, (7) NR data alternative representation, and (8) NR parameters of CGKRK/RSG interactions with CAN/PLA membranes.

Funding sources

AAA acknowledges funding from Kuwait University. RAC acknowledges funding from UKRI through the Engineering and Physical Sciences Research Council (UK) for support with grant EP/V029495/1.

CRediT authorship contribution statement

Abdulaziz A. Alobaid: Data curation, Formal analysis, Funding acquisition, Investigation, Methodology, Validation, Visualization, Writing – original draft, Writing – review & editing. **Maximilian W.A. Skoda:** Data curation, Formal analysis, Investigation, Methodology, Validation, Writing – review & editing. **Lynda K. Harris:** Conceptualization, Formal analysis, Funding acquisition, Methodology, Project administration, Resources, Supervision, Validation, Writing – original draft, Writing – review & editing. **Richard A. Campbell:** Conceptualization, Data curation, Formal analysis, Funding acquisition, Investigation, Methodology, Project administration, Resources, Supervision, Validation, Visualization, Writing – original draft, Writing – review & editing.

Declaration of competing interest

The authors declare that they have no known competing financial interests or personal relationships that could have appeared to influence the work reported in this paper.

Data availability

Data will be made available on request.

Acknowledgment

We thank the ISIS Neutron Source for beam time on the INTER reflectometer (DOI: 10.5286/ISIS.E.RB2010570) and Jayne Lawrence for helpful discussions.

Appendix A. Supplementary data

Supplementary data to this article can be found online at https://doi.org/10.1016/j.jcis.2024.02.103.

References

[1] F. Bray, J. Ferlay, I. Soerjomataram, R.L. Siegel, L.A. Torre, A. Jemal, Global cancer statistics 2018: GLOBOCAN estimates of incidence and mortality worldwide for 36 cancers in 185 countries, CA. Cancer J. Clin. 68 (6) (2018) 394–424.
[2] A.N. Giaquinto, H. Sung, K.D. Miller, J.L. Kramer, L.A. Newman, A. Minihan, A. Jemal, R.L. Siegel, Breast Cancer Statistics, 2022, CA Cancer J. Clin. 72 (6) (2022) 524–541.
[3] G. Ioele, M. Chieffallo, M.A. Occhiuzzi, M. De Luca, A. Garofalo, G. Ragno, F. Grande, Anticancer drugs: recent strategies to improve stability profile, pharmacokinetic and pharmacodynamic properties, Molecules 27 (17) (2022) 5436.
[4] S. Jin, Y. Sun, X. Liang, X. Gu, J. Ning, Y. Xu, S. Chen, L. Pan, Emerging new therapeutic antibody derivatives for cancer treatment, Signal Transd. Target. Ther. 7 (1) (2022) 39.
[5] T. Gholikhani, S. Kumar, H. Valizadeh, S. Mahdinloo, K. Adibkia, P. Zakeri-Milani, M. Barzegar-Jalali, B. Jimenez, Advances in aptamers-based applications in breast cancer: drug delivery, therapeutics, and diagnostics, Int. J. Mol. Sci. 23 (22) (2022) 14475.
[6] E. Ruoslahti, Vascular zip codes in angiogenesis and metastasis, Biochem. Soc. Trans. 32 (Pt3) (2004) 397–402.
[7] T. Teesalu, K. Sugahara, E. Ruoslahti, Tumor-penetrating peptides, Front. Oncol. 3 (2013) 216.
[8] A. Wada, T. Terashima, S. Kageyama, T. Yoshida, M. Narita, A. Kawauchi, H. Kojima, Efficient prostate cancer therapy with tissue-specific homing peptides identified by advanced phage display technology, Mol. Ther. Oncolytics 12 (2019) 138–146.
[9] D. Rajotte, W. Arap, M. Hagedorn, E. Koivunen, R. Pasqualini, E. Ruoslahti, Molecular heterogeneity of the vascular endothelium revealed by in vivo phage display, J. Clin. Invest. 102 (2) (1998) 430.
[10] L. Agemy, D. Friedmann-Morvinski, V.R. Kotamraju, L. Roth, K.N. Sugahara, O. M. Girard, R.F. Mattrey, I.M. Verma, E. Ruoslahti, Targeted nanoparticle enhanced proapoptotic peptide as potential therapy for glioblastoma, Proc. Natl. Acad. Sci. U S A 108 (42) (2011) 17450–17455.
[11] C. Ciobanasu, I. Dragomir, A. Apetrei, The penetrating properties of the tumor homing peptide LyP-1 in model lipid membranes, J. Pept. Sci. 25 (3) (2019) e3145.
[12] P. Lingasamy, T. Teesalu, Homing peptides for cancer therapy, Adv. Exp. Med. Biol. 1295 (2021) 29–48.
[13] L. Agemy, V.R. Kotamraju, D. Friedmann-Morvinski, S. Sharma, K.N. Sugahara, E. Ruoslahti, Proapoptotic peptide-mediated cancer therapy targeted to cell surface p32, Mol. Ther. 21 (12) (2013) 2195–2204.
[14] V. Costanzo, A. Bardelli, S. Siena, S. Abrignani, Exploring the links between cancer and placenta development, Open Biol. 8 (6) (2018).
[15] A. King, C. Ndifon, S. Lui, K. Widdows, V.R. Kotamraju, L. Agemy, T. Teesalu, J. D. Glazier, F. Cellesi, N. Tirelli, J.D. Aplin, E. Ruoslahti, L.K. Harris, Tumor-homing peptides as tools for targeted delivery of payloads to the placenta, Sci. Adv. 2 (5) (2016) e1600349.
[16] N. Cureton, I. Korotkova, B. Baker, S. Greenwood, M. Wareing, V.R. Kotamraju, T. Teesalu, F. Cellesi, N. Tirelli, E. Ruoslahti, J.D. Aplin, L.K. Harris, Selective targeting of a novel vasodilator to the uterine vasculature to treat impaired uteroplacental perfusion in pregnancy, Theranostics 7 (15) (2017) 3715–3731.
[17] L.J. Renshall, F. Beards, A. Evangelinos, S.L. Greenwood, P. Brownbill, A. Stevens, C.P. Sibley, J.D. Aplin, E.D. Johnstone, T. Teesalu, L.K. Harris, Targeted delivery of epidermal growth factor to the human placenta to treat fetal growth restriction, Pharmaceutics 13 (11) (2021) 1778.
[18] J.D. Aplin, J.E. Myers, K. Timms, M. Westwood, Tracking placental development in health and disease, Nat. Rev. Endocrinol. 16 (9) (2020) 479–494.
[19] G.J. Burton, E. Jauniaux, Pathophysiology of placental-derived fetal growth restriction, Am. J. Obstet. Gynecol. 218 (2s) (2018) 745–761.
[20] S. Rana, E. Lemoine, J.P. Granger, S.A. Karumanchi, Preeclampsia, Circ. Res. 124 (7) (2019) 1094–1112.
[21] S. Silva, A.J. Almeida, N. Vale, Combination of cell-penetrating peptides with nanoparticles for therapeutic application: a review, Biomolecules 9 (1) (2019) 22.
[22] P. Kapoor, H. Singh, A. Gautam, K. Chaudhary, R. Kumar, G.P. Raghava, TumorHoPe: a database of tumor homing peptides, Plos One 7 (4) (2012) e35187.
[23] T. Harayama, H. Riezman, Understanding the diversity of membrane lipid composition, Nat. Rev. Mol. Cell Biol. 19 (5) (2018) 281–296.
[24] W. Song, H.-Y. Yen, C.V. Robinson, M.S.P. Sansom, State-dependent lipid interactions with the A2a receptor revealed by MD simulations using in vivo-mimetic membranes, Structure 27 (2) (2019) 392–403.
[25] L. O'Neil, K. Andenoro, I. Pagano, L. Carroll, L. Langer, Z. Dell, D. Perera, B. W. Treece, F. Heinrich, M. Lösche, J.F. Nagle, S. Tristram-Nagle, HIV-1 matrix-31 membrane binding peptide interacts differently with membranes containing PS vs. PI(4,5)P2, Biochem. Biophys. Acta Biomembr. 1858 (12) (2016) 3071–3081.
[26] E.T. Castellana, P.S. Cremer, Solid supported lipid bilayers: From biophysical studies to sensor design, Surf. Sci. Reports 61 (10) (2006) 429–444.
[27] J. Daillant, E. Bellet-Amalric, A. Braslau, T. Charitat, G. Fragneto, F. Graner, S. Mora, F. Rieutord, B. Stidder, Structure and fluctuations of a single floating lipid bilayer, Proc. Natl. Acad. Sci. U S A 102 (33) (2005) 11639–11644.
[28] L.A. Clifton, R.A. Campbell, F. Sebastiani, J. Campos-Terán, J.F. Gonzalez-Martinez, S. Björklund, J. Sotres, M. Cárdenas, Design and use of model membranes to study biomolecular interactions using complementary surface-sensitive techniques, Adv. Colloid Interface Sci. 277 (2020) 102118.
[29] D. Ciumac, R.A. Campbell, H. Xu, L.A. Clifton, A.V. Hughes, J.R.P. Webster, J. R. Lu, Implications of lipid monolayer charge characteristics on their selective interactions with a short antimicrobial peptide, Colloids Surf. B: Biointerfaces 150 (2017) 308–316.
[30] A.P. Le Brun, C.L. Haigh, S.C. Drew, M. James, M.P. Boland, S.J. Collins, Neutron reflectometry studies define prion protein n-terminal peptide membrane binding, Biophys. J. 107 (10) (2014) 2313–2324.
[31] A. Luchini, F.G. Tidemand, N.T. Johansen, F. Sebastiani, G. Corucci, G. Fragneto, M. Cárdenas, L. Arleth, Dark peptide discs for the investigation of membrane proteins in supported lipid bilayers: the case of synaptobrevin 2 (VAMP2), Nanoscale Adv. 4 (21) (2022) 4526–4534.
[32] L.A. Clifton, F. Ciesielski, M.W.A. Skoda, N. Paracini, S.A. Holt, J.H. Lakey, The effect of lipopolysaccharide core oligosaccharide size on the electrostatic binding of antimicrobial proteins to models of the gram negative bacterial outer membrane, Langmuir 32 (14) (2016) 3485–3494.
[33] L. Ma, Y. Luo, Y.-H. Ma, X. Lu, Interaction between antimicrobial peptide CM15 and a model cell membrane affected by CM15 terminal amidation and the membrane phase state, Langmuir 37 (4) (2021) 1613–1621.
[34] M. He, S. Guo, Z. Li, In situ characterizing membrane lipid phenotype of breast cancer cells using mass spectrometry profiling, Sci. Reports 5 (1) (2015) 11298.
[35] L. Levi, M. Castro-Parodi, N. Martínez, L.L. Piehl, E. Rubín De Celis, V. Herlax, S. Mate, M. Farina, A.E. Damiano, The unfavorable lipid environment reduced caveolin-1 expression in apical membranes from human preeclamptic placentas, Biochim. Biophys. Acta. Biomembr. 1858 (9) (2016) 2171–2180.
[36] D. Marsh, Comment on interpretation of mechanochemical properties of lipid bilayer vesicles from the equation of state or pressure–area measurement of the

monolayer at the air−water or oil−water interface, Langmuir 22 (6) (2006) 2916–2919.
[37] S. Galdiero, A. Falanga, M. Cantisani, M. Vitiello, G. Morelli, M. Galdiero, Peptide-lipid interactions: experiments and applications, Int. J. Mol. Sci. 14 (9) (2013) 18758–18789.
[38] Bachem, Peptide calculator. https://www.bachem.com/knowledge-center/peptide-calculator/. (Accessed May 2023).
[39] L. Gkionis, R.A. Campbell, H. Aojula, L.K. Harris, A. Tirella, Manufacturing drug co-loaded liposomal formulations targeting breast cancer: Influence of preparative method on liposomes characteristics and in vitro toxicity, Int. J. Pharm. 590 (2020) 119926.
[40] A. Casadó, M.C. Giuffrida, M.L. Sagristá, F. Castelli, M. Pujol, M.A. Alsina, M. Mora, Langmuir monolayers and Differential Scanning Calorimetry for the study of the interactions between camptothecin drugs and biomembrane models, Biochim. Biophys. Acta Biomembr. 1858 (2) (2016) 422–433.
[41] R. Maget-Dana, D. Lelièvre, Comparative interaction of alpha-helical and beta-sheet amphiphilic isopeptides with phospholipid monolayers, Biopolymers 59 (1) (2001) 1–10.
[42] J. Humlíček, 1 - Polarized Light and Ellipsometry, in: H.G. Tompkins, E.A. Irene (Eds.), Handbook of Ellipsometry, William Andrew Publishing, Norwich, NY, 2005, pp. 3–91.
[43] M.-L. Ainalem, R.A. Campbell, T. Nylander, Interactions between DNA and poly (amido amine) dendrimers on silica surfaces, J. Am. Chem. Soc 26 (11) (2010) 8625–8635.
[44] A. Spadea, M. Jackman, L. Cui, S. Pereira, M.J. Lawrence, R.A. Campbell, M. Ashford, Nucleic acid-loaded lipid nanoparticle interactions with model endosomal membranes, ACS Appl. Mater. Interfaces 14 (26) (2022) 30371–30384.
[45] W. Daear, M. Mahadeo, E.J. Prenner, Applications of Brewster angle microscopy from biological materials to biological systems, Biochim. Biophys. Act Biomembr. 1859 (10) (2017) 1749–1766.
[46] T. Charitat, E. Bellet-Amalric, G. Fragneto, F. Graner, Adsorbed and free lipid bilayers at the solid-liquid interface, Euro. Phys. J. B 8 (4) (1999) 583–593.
[47] R.A. Campbell, Recent advances in resolving kinetic and dynamic processes at the air/water interface using specular neutron reflectometry, Curr. Opin. Colloid Interface Sci. 37 (2018) 49–60.
[48] M.W.A. Skoda, Recent developments in the application of X-ray and neutron reflectivity to soft-matter systems, Curr. Opin. Colloid Interface Sci. 42 (2019) 41–54.
[49] A. Nelson, Co-refinement of multiple-contrast neutron/X-ray reflectivity data using MOTOFIT, J. Appl. Crystallog. 39 (2) (2006) 273–276.
[50] A. Braslau, M. Deutsch, P.S. Pershan, A.H. Weiss, J. Als-Nielsen, J. Bohr, Surface roughness of water measured by X-ray reflectivity, Phys. Rev. Lett. 54 (2) (1985) 114–117.
[51] R.A. Campbell, Y. Saaka, Y. Shao, Y. Gerelli, R. Cubitt, E. Nazaruk, D. Matyszewska, M.J. Lawrence, Structure of surfactant and phospholipid monolayers at the air/water interface modeled from neutron reflectivity data, J. Colloid Interfaces Sci. 531 (2018) 98–108.
[52] L.A. Clifton, M.R. Sanders, A.V. Hughes, C. Neylon, R.A. Frazier, R.J. Green, Lipid binding interactions of antimicrobial plant seed defence proteins: puroindoline-a and β-purothionin, Phys. Chem. Chem. Phys. 13 (38) (2011) 17153–17162.
[53] D.P. Hoogerheide, S.Y. Noskov, D. Jacobs, L. Bergdoll, V. Silin, D.L. Worcester, J. Abramson, H. Nanda, T.K. Rostovtseva, S.M. Bezrukov, Structural features and lipid binding domain of tubulin on biomimetic mitochondrial membranes, Proc. Natl. Acad. Sci. U S A 114 (18) (2017) 3622–3631.
[54] J.A. Hoffman, E. Giraudo, M. Singh, L. Zhang, M. Inoue, K. Porkka, D. Hanahan, E. Ruoslahti, Progressive vascular changes in a transgenic mouse model of squamous cell carcinoma, Cancer Cell 4 (5) (2003) 383–391.
[55] Y. Ma, S.K. Ghosh, D.A. DiLena, S. Bera, L.B. Lurio, A.N. Parikh, S.K. Sinha, Cholesterol partition and condensing effect in phase-separated ternary mixture lipid multilayers, Biophys. J. 110 (6) (2016) 1355–1366.
[56] G.P. Connelly, Y. Bai, M.-F. Jeng, S.W. Englander, Isotope effects in peptide group hydrogen exchange, Proteins: Struct. Funct. Bioinfo. 17 (1) (1993) 87–92.
[57] L. Braun, M. Uhlig, O. Löhmann, R.A. Campbell, E. Schneck, R. von Klitzing, Insights into extended structures and their driving force: influence of salt on polyelectrolyte/surfactant mixtures at the air/water interface, ACS Appl. Mater. Interfaces 14 (23) (2022) 27347–27359.
[58] D. Matyszewska, E. Nazaruk, R.A. Campbell, Interactions of anticancer drugs doxorubicin and idarubicin with lipid monolayers: New insight into the composition, structure and morphology, J. Colloid Interface Sci. 581 (2021) 403–416.
[59] M.-L. Jobin, P. Bonnafous, H. Temsamani, F. Dole, A. Grélard, E.J. Dufourc, I. D. Alves, The enhanced membrane interaction and perturbation of a cell penetrating peptide in the presence of anionic lipids: Toward an understanding of its selectivity for cancer cells, Biochim. Biophys. Acta Biomembr. 1828 (6) (2013) 1457–1470.
[60] N.A. Alhakamy, P. Dhar, C.J. Berkland, Charge type, charge spacing, and hydrophobicity of arginine-rich cell-penetrating peptides dictate gene transfection, Mol. Pharm. 13 (3) (2016) 1047–1057.
[61] S. Trabulo, A.L. Cardoso, M. Mano, M.C.P. De Lima, Cell-penetrating peptides—mechanisms of cellular uptake and generation of delivery systems, Pharmaceuticals 3 (4) (2010) 961–993.
[62] E. Ruoslahti, S.N. Bhatia, M.J. Sailor, Targeting of drugs and nanoparticles to tumors, J. Cell Biol. 188 (6) (2010) 759–768.
[63] M.N. O'Brien, M.R. Jones, C.A. Mirkin, The nature and implications of uniformity in the hierarchical organization of nanomaterials, Proc. Natl. Acad. Sci. U S A 113 (42) (2016) 11717–11725.
[64] J.I. Griffin, S.K.K. Cheng, T. Hayashi, D. Carson, M. Saraswathy, D.P. Nair, D. Simberg, Cell-penetrating peptide CGKRK mediates efficient and widespread targeting of bladder mucosa following focal injury, Nanomedicine 13 (6) (2017) 1925–1932.
[65] D.M. Copolovici, K. Langel, E. Eriste, Ü. Langel, Cell-penetrating peptides: design, synthesis, and applications, ACS Nano 8 (3) (2014) 1972–1994.
[66] H. Gong, X. Hu, L. Zhang, K. Fa, M. Liao, H. Liu, G. Fragneto, M. Campana, J.R. Lu, How do antimicrobial peptides disrupt the lipopolysaccharide membrane leaflet of Gram-negative bacteria? J. Colloid Interface Sci. 637 (2023) 182–192.
[67] P. Gehan, S. Kulifaj, P. Soule, J.B. Bodin, M. Amoura, A. Walrant, S. Sagon, A. R. Thiam, K. Ngo, V. Vivier, S. Cribier, N. Rodriguez, Penetratin translocation mechanism through asymmetric droplet interface bilayers, Biochim. Biophys. Acta Biomembr. 1862 (2020) 183415.
[68] N.A. Alhakamy, A.L. Alaofi, O.A.A. Ahmed, U.A. Fahmy, S. Md, W.H. Abdulaal, M. A. Alfaleh, A. Chakraborty, C.J. Berkland, P. Dhar, Development of lipid membrane based assays to accurately predict the transfection efficiency of cell-penetrating peptide-based gene nanoparticles, Int. J. Pharm. 580 (2020) 119221.
[69] R. Hadianamrei, M.A. Tomeh, S. Brown, J. Wang, X. Zhao, Rationally designed short cationic α-helical peptides with selective anticancer activity, J. Colloid Interface Sci. 607 (2022) 488–501.
[70] F.G. Avci, B.S. Akbulut, E. Ozkirimli, Membrane active peptides and their biophysical characterization, Biomolecules 8 (3) (2018) 77.
[71] H.C. Geisler, H.C. Safford, M.J. Mitchell, Rational design of nanomedicine for placental disorders: birthing a new era in women's reproductive health, Small (2023) 2300852.
[72] F. Madani, A. Gräslund, Investigating membrane interactions and structures of CPPs, Methods Mol. Biol. 1324 (2015) 73–87.